INTERNATIONAL ATOMIC ENERGY AGENCY
UNITED NATIONS EDUCATIONAL, SCIENTIFIC AND CULTURAL ORGANIZATION
INTERNATIONAL CENTRE FOR THEORETICAL PHYSICS
I.C.T.P., P.O. BOX 586, 34100 TRIESTE, ITALY, CABLE: CENTRATOM TRIESTE

H4.SMR/782-15

Second Workshop on Three-Dimensional Modelling of Seismic Waves Generation, Propagation and their Inversion

7 - 18 November 1994

Surface-wave Group Velocity Tomography of East Asia

F.T. Wu* - A. Levshin**

* State University of New York
Department of Geological Sciences
Binghamton, New York
U.S.A.

**University of Colorado
Department of Physics
Boulder, Colorado
U.S.A.

Reprinted from

PHYSICS OF THE EARTH AND PLANETARY INTERIORS

Physics of the Earth and Planetary Interiors 84 (1994) 59–77

Surface-wave group velocity tomography of East Asia

Francis T. Wu *,[a], Anatoli Levshin [b]

[a] *Department of Geological Sciences, State University of New York, Binghamton, NY 13902-6000, USA*
[b] *Joint Seismic Program Center, Department of Physics, University of Colorado, Boulder, CO 80390-0390, USA*

(Received 1 January 1993; revision accepted 8 December 1993)

PHYSICS OF THE EARTH AND PLANETARY INTERIORS

Scope of the Journal

Physics of the Earth and Planetary Interiors will be devoted to the application of chemistry and physics to studies of the Earth's crust, mantle and core and to the interiors of the planets. It is hoped that it will attract papers of high originality and, with an international coverage, contribute to the sound development of this well-established field of the Earth and Space Sciences. Types of contributions to be published are: (1) research papers; (2) reviews; (3) short communications, preferably in the *Letter Section* (see Note to Contributors on the back inside cover); (4) discussions; (5) book reviews; and (6) announcements.

Publication Information

Physics of the Earth and Planetary Interiors (ISSN 0031-9201). For 1994 volumes 81–86 are scheduled for publication.

Subscription prices are available upon request from the Publisher. Subscriptions are accepted on a prepaid basis only and are entered on a calendar year basis. Issues are sent by surface mail except to the following countries where air delivery via SAL mail is ensured: Argentina, Australia, Brazil, Canada, Hong Kong, India, Israel, Japan, Malaysia, Mexico, New Zealand, Pakistan, P.R. China, Singapore, South Africa, South Korea, Taiwan, Thailand, USA. For all other countries airmail rates are available upon request.

Claims for missing issues must be made within six months of our publication (mailing) date.

Please address all your requests regarding orders and subscription queries to: Elsevier Science B.V., Journal Department, P.O. Box 211, 1000 AE Amsterdam, Netherlands, tel. 31-20-5803642, fax 31-20-5803598.

For further information, or a free sample copy of this or any other Elsevier Science journal, readers in the USA and Canada can contact the following address: Elsevier Science Inc., Journal Information Center, 655 Avenue of the Americas, New York, NY 10010, USA, tel. (212) 633-3750, fax (212) 633-3764.

All back volumes, except Vols. 5 and 14 are available. Price per volume: Dfl. 321.00 (approx. US$183.40), inclusive of postage, packing and handling. Orders and information requests should be addressed to Elsevier Science B.V., Special Services Department, P.O. Box 211, 1000 AE Amsterdam, Netherlands. *All back volumes are available on microfilm*. Orders and information requests concerning back volumes on microfilm should be addressed exclusively to: Elsevier Science S.A., P.O. Box 851, 1001 Lausanne, Switzerland.

US mailing notice — *Physics of the Earth and Planetary Interiors* (ISSN 0031-9201) is published monthly by Elsevier Science B.V., (Molenwerf 1, Postbus 211, 1000 AE Amsterdam). Annual subscription price in the USA US$ 1317.00 (valid in North, Central and South America only), including air speed delivery. Second class postage rate paid at Jamaica, NY 11431.
USA POSTMASTERS: Send address changes to *Physics of the Earth and Planetary Interiors* Publications Expediting, Inc., 200 Meacham Avenue, Elmont, NY 11003.
Airfreight and mailing in the USA by Publications Expediting.

ELSEVIER

Physics of the Earth and Planetary Interiors 84 (1994) 59–77

PHYSICS OF THE EARTH AND PLANETARY INTERIORS

Surface-wave group velocity tomography of East Asia

Francis T. Wu *,[a], Anatoli Levshin [b]

[a] *Department of Geological Sciences, State University of New York, Binghamton, NY 13902-6000, USA*
[b] *Joint Seismic Program Center, Department of Physics, University of Colorado, Boulder, CO 80390-0390, USA*

(Received 1 January 1993; revision accepted 8 December 1993)

Abstract

Group velocities of both Rayleigh and Love waves are used in a tomographic inversion to obtain group velocity maps of East Asia (60–140°E and 20–60°N). The period range studied is 30–70 s. The Tibetan plateau, a region undergoing intense north–south compression, appears as a prominent low-velocity (about −15% from the average) structure in this area; central Tibet appears as the area with the lowest velocities, and southern Tibet, south of the Zangbo suture zone and the Himalayas, is an area of high velocities. The Tibet low-velocity area extends northward to the southern Tarim basin. The North China–Korean platform, an area traditionally recognized as the oldest platform in China, does not have a consistent crust and upper-mantle velocity signature. The North China plain, a part of the platform where extensional tectonics dominates, is an area of high velocities, probably as a result of thin crust. The other parts of the platform have relatively low velocities. The south China block, the least tectonically active region of China, is generally an area of high velocity. For periods longer than 40 s, a high group velocity gradient clearly exists along longitude 105°E; the velocities are noticeably higher east of this longitude than west of it. This transition corresponds closely to that in the Bouguer gravity map. In general, processes in the crust and upper mantle owing to recent tectonic activities, rather than the age of the basement rocks, seem to have dominant control of crust and upper-mantle velocity structures.

1. Introduction

The purpose of this study is to image the lateral variations of crust and upper-mantle structures in East Asia. Seismic surface-wave group velocity is chosen as the datum because it is relatively easy to obtain a dense distribution of paths using the events in and on the periphery of the study area and the high-quality digital seismic stations in China and the surrounding areas.

East Asia is a region of complex topography and tectonics. As shown in Fig. 1, the Tibet–Pamir plateau is the dominant topographic feature. Whereas the descent from the Tibetan plateau southward to the northern Indian plain is very rapid, the transition to lower elevations in the other directions, especially toward the north and the northeast, is more gradual. Large basins and mountain chains intersperse. As shown in Fig. 1, the tectonic units are often associated with certain topographic characteristics.

It is widely recognized that the southern border of Tibet is a collision boundary (Molnar and

* Corresponding author.

Elsevier Science B.V.
SSDI 0031-9201(94)05026-T

Tapponnier, 1978), with the Indian plate underthrusting toward the north. The area of active intraplate tectonics north and northeast of Tibet extends thousands of kilometers, over terranes with diverse tectonic history. The oldest part of the continent of Asia, the Angara craton, lies far away from Tibet, in Siberia (Fig. 1). This craton is considered to be the core around which the continent grew throughout geological time, as a result of successive accretions of younger terranes onto it (Sengor et al., 1993). The tectonic units to the south are generally younger. The Altaid tectonic collage (Fig. 1) surrounding the core is possibly a giant subduction–accretion complex formed during the Paleozoic era. The southern boundary of this complex consists of a series of mountains: the Tienshan in Kyrgyzstan and western China, to the north of the Tarim basin, continues eastward to the Beishan near the Mongolian border and the Yinshan in northeastern China; this chain is a part of a Paleozoic suture. Along this chain, the western Tienshan is a very active compressive tectonic belt, but the eastern Tienshan, where a deep east–west intermontane basin is situated, is much less so. To the south of the Altaids is the North China–Korean platform, composed of a series of Precambrian blocks, the Tarim, the Ala Shan, the Ordos and North China plain (Fig. 1); these blocks appear to be relatively rigid and are not tectonically active at present, but they are separated by active structures. The North China–Korean platform is the oldest platform

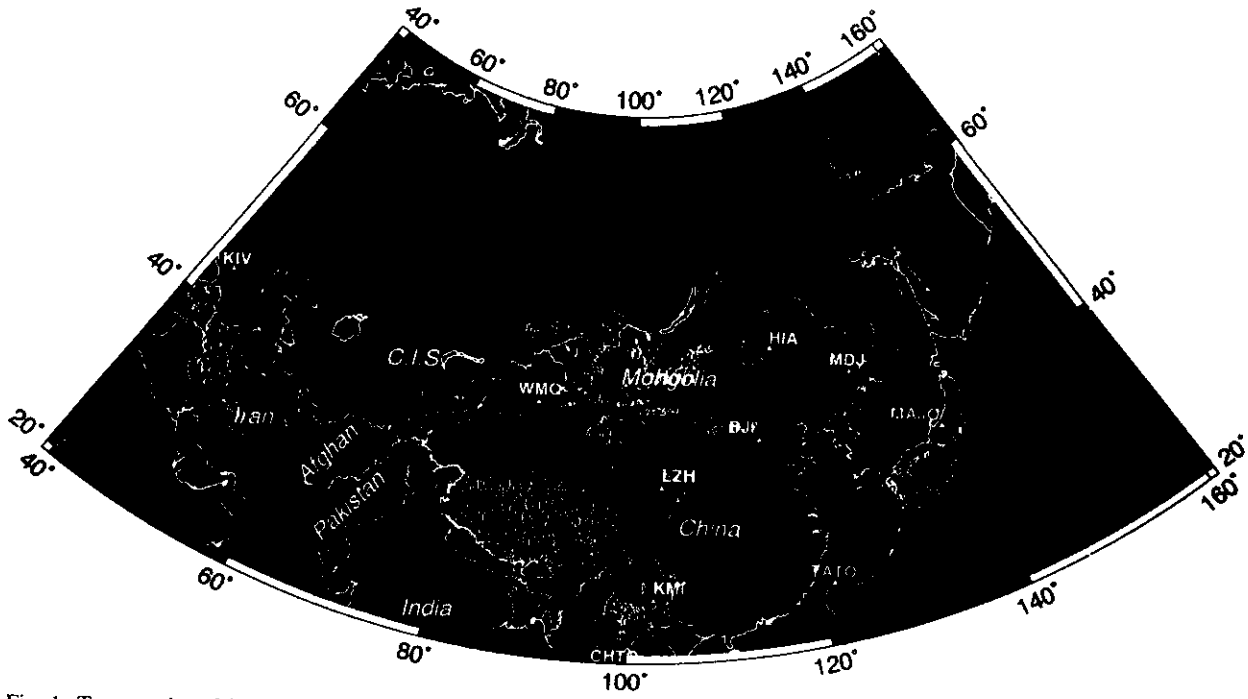

Fig. 1. Topography of East Asia based on the ETOPO5 topographic database with generalized tectonics superimposed (after Terman (1973) and Sengor et al. (1993)). The numbered features are: (1) North China plain; (2) Ordos platform; (3) Ala Shan block; (4) Tarim basin (these four, together with North Korea, are often collectively called the North China–Korean platform); (5) Qaidam basin; (6) Tibetan plateau; (7) Sichuan basin; (8) South China platform; (9) Sung-Liau plain; (10) Tienshan The locations of seismic stations used in the study are shown as triangles. Station CHTO is below latitude 20° at longitude 100°E. (Note that many of the tectonic units shown in Fig. 1 are clearly associated with major topographical features.) The Tibetan plateau is the most prominent feature on this map. Some of the somewhat subtle features can be seen in this map. For example, although the eastern section of the Tienshan southeast of Station WMQ is a continuation of the western Tienshan, it is actually a basin and range area with its lowest point in the Turfan basin (−280 m). The Sichuan basin (7), the red area north of Station KMI) is surrounded by 1000–2000 m mountain ranges. The change in topography eastward from western China is unshaded.

covered by our group velocity maps. South of this platform is the Paleozoic–Mesozoic suture along the Kunlun and the Astin Tagh chains, north of the Tibetan plateau, the Nanshan (north of the Qaidam basin) and Qinling of eastern China; with the exception of Qinling, this suture has been reactivated. South China was evidently attached to the rest of Asia in Permian times, and it is one of the least active areas in China, except at its southeastern edge, especially near Taiwan, where collision between the Eurasian and the Philippine plates is taking place (Wu, 1978). Further to the west, the southern Tibetan block was accreted to northern Tibet in the early Mesozoic and the suturing of the Indian plate to the Eurasian plate along the Himalayan front, which started about 50 m.y. ago, led to the formation of Tibet and the continuing continental tectonics of the whole East Asian area (Molnar and Tapponnier, 1978).

There have been a number of studies using body or surface waves to investigate the crust and upper-mantle structures of the area. These results provide important clues for the interpretation of our results in several regions. A limited number of crustal reflection and refraction profiles in various parts of China were obtained by Chinese groups (see Wang and Mao (1985) for a summary). By far the most detailed surveys were done in the North China plain, near Beijing, in conjunction with earthquake studies. Several refraction and wide-angle reflection studies were done in southern Tibet (Wang and Mao, 1985; Hirn, 1988). In general, the studies above were aimed at obtaining details of structures along profiles, but the lateral changes in velocity and crustal thickness in the various regions were not mapped by such studies.

Surface waves from earthquakes can be used to obtain average structures along their travel paths. Also, using a large number of paths traversing a laterally varying region with sufficient azimuthal coverage, tomographic inversion can be used to construct a group or phase velocity image of the region. With the exceptions of a study of southern Tibet by Jobert et al. (1985), a two-station Rayleigh dispersion study of several regions of China by Feng et al. (1983), a Rayleigh group velocity study by Kozhevnikov et al. (1992) and a tomographic study of Tibet by Bourjot and

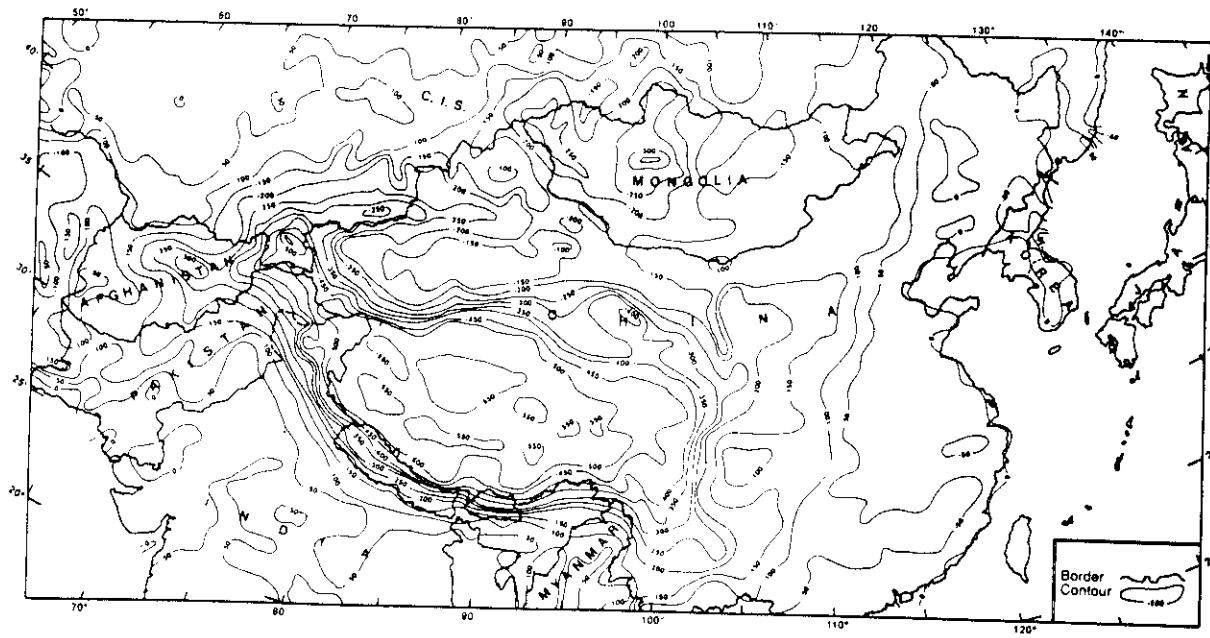

Fig. 2. Simplified Bouguer gravity map of the study area (USAF, 1971). (Note the −550 mgal anomalies in Tibet, the relative high over the Tarim basin, and the continuous increase toward the east.)

Romanowicz (1992), most of the previous surface-wave studies in East Asia were done with data external to the region of interest. Feng et al. (1983) used data recorded on Kirnos seismographs from stations within China to derive Rayleigh wave dispersion in the period range of 10–50 s. Relatively few paths were used in their study. Patton (1980) and Feng and Teng (1983) obtained dispersion curves for various areas of Eurasia with Rayleigh waves traversing the area by regionalization. Whereas Patton (1980) defined the sub-regions based on topography and known crustal thickness, Feng and Teng (1983) divided the region into 10° × 10°grids; the paths used are relatively sparse because of the scarcity of data and the resolution is rather coarse because of the grid size. Wier (1982) determined group velocities for the eastern part of China along several paths using three Seismic Research Observatory (SRO) stations. Chun and Yoshii (1977) used events on the eastern side of the Tibetan plateau and stations south of the Himalayas; their study was focused on Tibet. Brandon and Romanowicz (1986) employed the 'two-event' technique to determine dispersion curves in northern Tibet. Kozhevnikov and Barmin (1989) analyzed about 200 records of analog Soviet stations and several SRO stations deployed in Asia to obtain average Rayleigh wave group velocity curves for several predetermined tectonic regions of Eastern Asia. These curves were used by Kozhevnikov et al. (1992) to find average lithosphere shear-velocity structure for Tibet, the mountain region of Southern Siberia and Mongolia, platforms of south-eastern China and some other regions. Bourjot and Romanowicz (1992) recently presented tomographic images of the Tibetan plateau and its vicinity; they used two stations in China, several SRO stations in Asia, and also ANTO in Turkey, GRFO in Germany and SSB in France.

For large-scale lateral variations in crustal structures in Asia, the Bouguer gravity map of this region (US Air Force (USAF), 1971) provides additional constraints (Fig. 2). The most prominent anomalies on this map are over the Tibetan plateau, where they are as low as −550 mgal. The overall trend of anomalies shown on the map is a general decrease in the amplitude of the negative anomalies toward the east. We shall see later in our discussion that many details of this map correlate fairly closely with the group velocity images obtained in this study.

Our tomographic study was made possible by the establishment of high-quality seismic stations in China and its vicinity. Although the network is still too sparse, with station spacing of the order of 1000 km, by using data from six stations of the Chinese Digital Seismic Network (CDSN) and three stations of the SRO network (see Fig. 1 for station distribution) and earthquakes larger than $M = 4.7$ in this region or on its periphery, we are able to perform this study with 3 years of data. Group velocity is used because we want to maximize our paths for better resolution and most of the events are too small to have dependable focal mechanisms, without which we cannot obtain reliable phase velocities with single stations.

The method used in our tomographic inversion was developed by Ditmar and Yanovskaya (1987; see also Levshin et al., 1989). For each period, a smooth group velocity image is obtained, with its spatial resolution (in km) depending on the distribution of raypaths. The tomographic images of the region as a whole, using Rayleigh and Love wave dispersion curves, show clearly the lateral variations in crustal and upper-mantle structures. Although Tibet is by far the most prominent feature in the region, we are also able to resolve many smaller features in East Asia. Of particular interest is the effect of recent tectonics on geologically ancient terranes, as many of the structures have been rejuvenated in the recent episode of tectonic activities.

2. Data

Fig. 1 shows the locations of the CDSN and SRO stations and many of the events used in this study. Because of the wide dynamic range of the CDSN and the upgraded SRO seismic systems, the records stay on scale for Magnitude 7 earthquakes, and, in some cases, surface waves from $M_S \approx 4.3$ events are recorded with such good signal-to-noise ratio that they can be used to deter-

mine group velocities in the 20–70 s range. Altogether, 100 events that occurred in 1987, the first 6 months of 1989, 1990 and the first half of 1991, were used; the time spans used are related to the availability of data when they were acquired. The events chosen are located in and on the periphery of the study area. Of the 500 event–station paths, approximately 360 Love and 360 Rayleigh dispersion curves were retained for the final analyses. The group velocity dispersion curves were determined with an interactive multiple filter group velocity program on a workstation, allowing rapid group velocity determination and visual quality control. Dispersion data are discarded when the sonogram shows complex envelope structures along the group arrival. In such cases, we note that the waveform is usually more complex and relatively small; such waves are probably radiated near the radiation pattern minimum and thus multipathing effects become pronounced.

Because of the relatively short path length used in our study, the effect of instrument group delay is not negligible in the determination of group velocities. McCowan and Lacoss (1978) have shown that SRO instruments have delays ranging from about 12 s at a period of 20 s to about 24 s at a period of 70 s (without anti-aliasing filter). For the CDSN long-period channels the group delays ranges from 15 s at a period of 20 s to 35 s at a period of 30 s. With the path lengths varying from 1000 to 4000 km, neglecting group delays can lead to an error of several per cent to 10%. Fig. 3 summarizes the group delays of the SRO, CDSN and the modified SRO instruments (MAJO2) used in this study. Broadband instruments, such as those used now at MAJO, have relatively small group delay.

3. Tomographic method

To invert surface-wave group velocities we applied a technique developed by Ditmar and Yanovskaya (1987) and Yanovskaya and Ditmar

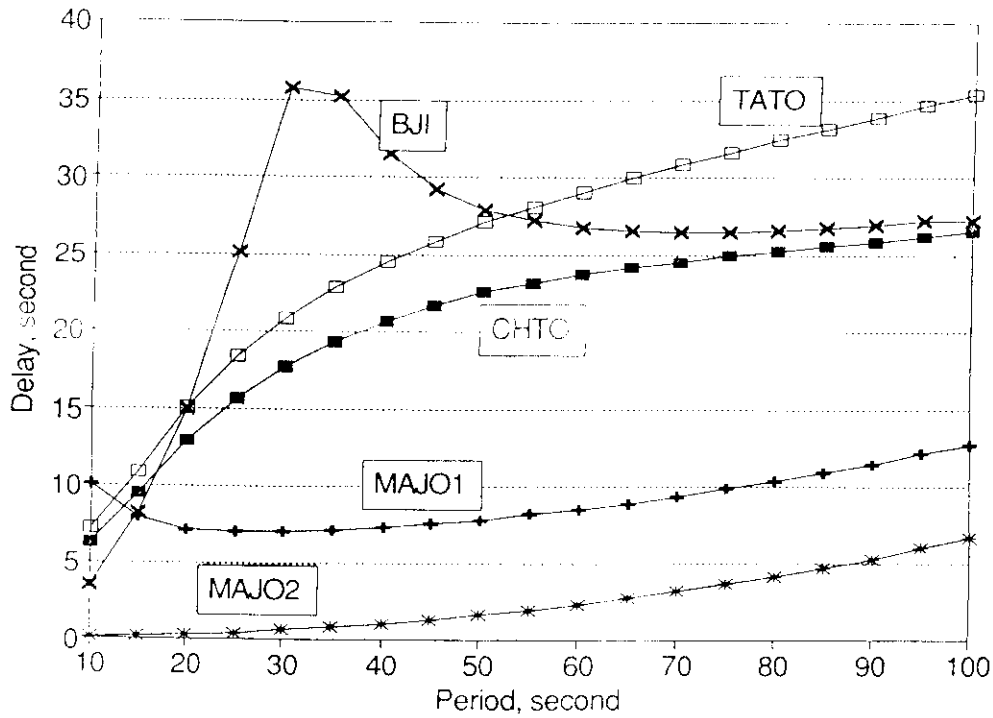

Fig. 3. Instrument group delays for World Wide Standard Seismograph Network (WWSSN), Chinese Digital Seismic Network (CDSN), Seismic Research Observatory (SRO) instruments at TATO (from 28 August 1980 to mid-1992) and MAJO (MAJO1 for 23 August 1988–20 August 1990, MAJO2 for 20 August 1990–8 February 1991).

(1990). This technique can be considered a generalization of the Backus–Gilbert inversion method (Backus and Gilbert, 1968, 1970) for 2D problems. Input data for inversion are group travel times t_j for several fixed values T_m, $m = 1, \ldots, M$, of period T along given paths L_j, $j = 1, \ldots, J$, and corresponding cross-correlation matrices of travel time errors, $R_t \mid_T = T_m$. Results of inversion are maps of group velocity distribution $U(\theta, \phi) \mid_T = Tm$ and a map of space resolution $R(\theta\phi)$ for a given set of paths. Here θ and ϕ are latitude and longitude, respectively. The inversion procedure will be repeated for each period of interest.

Let the real distribution of group velocities be $U_e(\theta, \phi)$. To obtain a tomographic image of it we use a laterally homogeneous initial model of the area S under study with a constant group velocity U_0. The basic assumptions of the inversion technique are as follows:

(1) deviations of the real distribution of velocities from the starting model are small, i.e.

$$m_e(\theta, \phi) = \left[U_e^{-1}(\theta, \phi) - U_0^{-1} U_0\right] \ll 1 \qquad (1)$$

so that we can ignore the deviations of wave paths from great circles and, also, use linearized inversion procedures.

(2) Taking into account incompleteness and inaccuracy of the data set, we are looking for a smooth image $m(\theta, \phi)$ of the real velocity perturbations relative to the starting model. To do this, we introduce constraints

$$\int_S |\nabla m(r)|^2 \, \mathrm{d}r = \min \qquad (2)$$

and

$$\left(\frac{\partial m}{\partial n}\right) C_S = 0 \qquad (3)$$

Here C_S is a contour surrounding the area S and n is a normal to C_S.

(3) The solution obeys constraints related to data

$$\int_S G_i(r) m(r) \, \mathrm{d}r = \int_{L_i} m(s) U_0^{-1} \, \mathrm{d}s = \delta t_i \qquad (4)$$

$$t_{0i} = \int_{L_i} U_0^{-1} \, \mathrm{d}s \qquad (5)$$

Here G_i is a data kernel singular along the path L_i, equal to zero outside the path and obeying the relationship

$$\int_S G_i(r) \, \mathrm{d} = t_{0i} \qquad (6)$$

$$\delta t_i \approx t_i - t_{0i} = \int_{L_i} m(s) U_0^{-1} \, \mathrm{d}s \qquad (7)$$

Using the regularization technique (Tikhonov and Arsenin, 1976) in the case of inaccurate data it is possible to state the problem of searching for a solution as finding the minimum of the following functional:

$$(\delta t - P)^T R_t^{-1} (\delta t - P) + \alpha \int_S |\nabla m(r)|^2 \, \mathrm{d}r = \min \qquad (8)$$

Here $P_i = \int_S G_i(r) m(r) \mathrm{d}r$ and α is a regularization parameter. α must be chosen so that the first term in (8) is equal to the total number N of data. By increasing α we impose stronger smoothness and decrease the resolving power of data.

The solution $m(\theta, \phi)$ is found using the formulae

$$m = A^T \delta t \qquad (9)$$

Table 1
Inversion parameter and residuals for Love and Rayleigh waves, for various periods

Period (s)	No. of paths	Av. velocity (km s^{-1})	Av. residual (s)
Love waves			
30	358	3.35	27.2
40	357	3.52	25.7
50	357	3.67	27.8
60	349	3.82	32.8
70	344	3.93	40.1
Rayleigh waves			
30	362	3.08	28.2
40	362	3.30	23.7
50	362	3.48	24.0
60	362	3.61	21.0
70	361	3.70	21.9

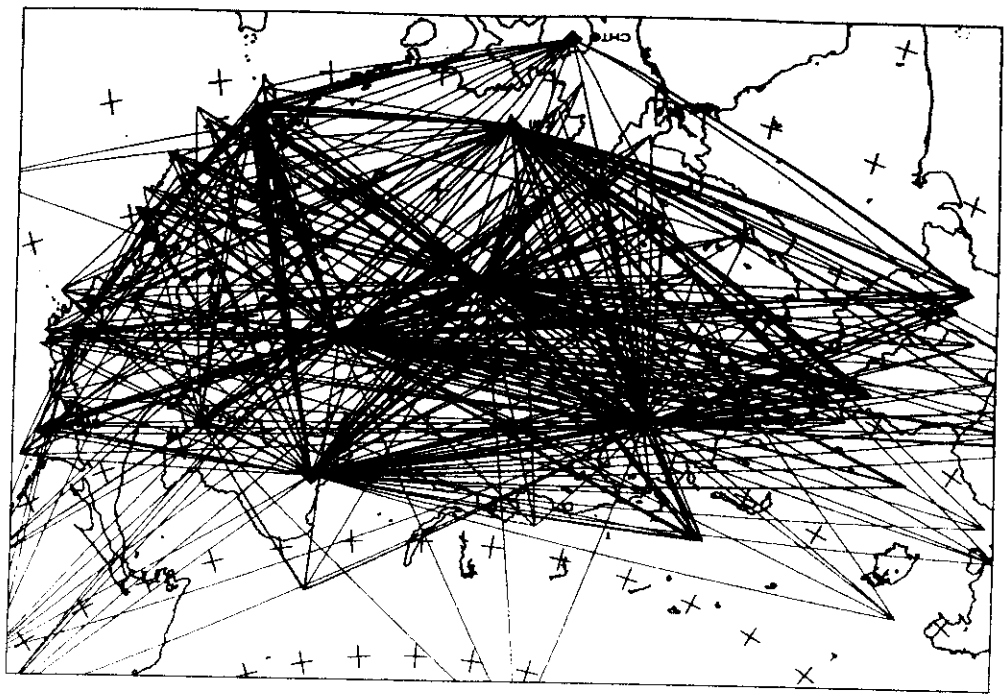

(a)

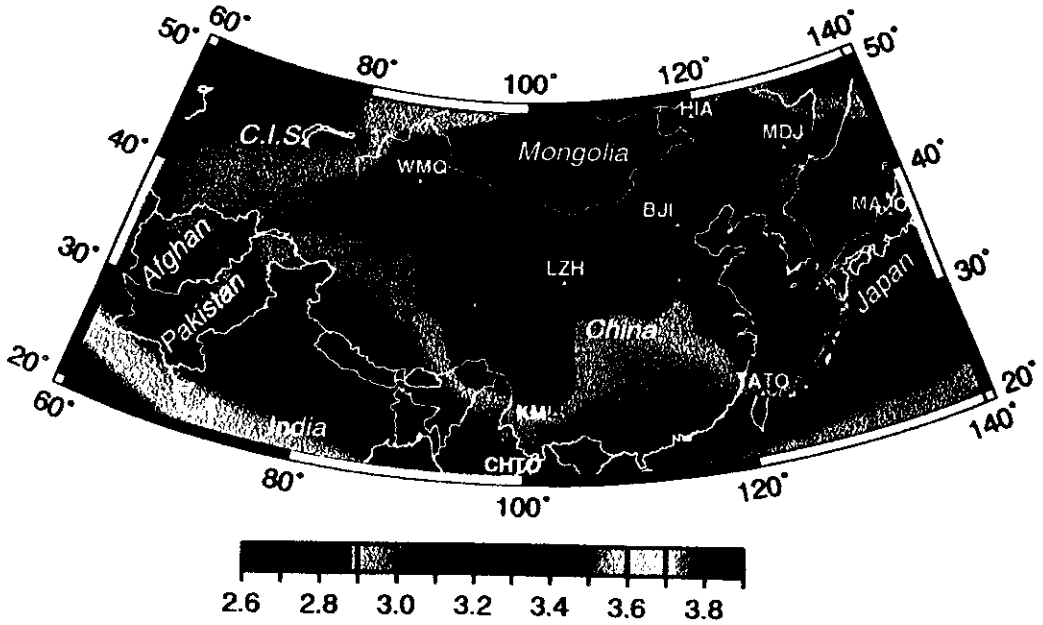

(b)

Fig. 4. (a) Path coverage for this study. Along most of the paths both Love and Rayleigh waves are available. For different periods the coverage varies slightly. (b) Resolution of tomographic inversion results for Rayleigh waves at 50 s.

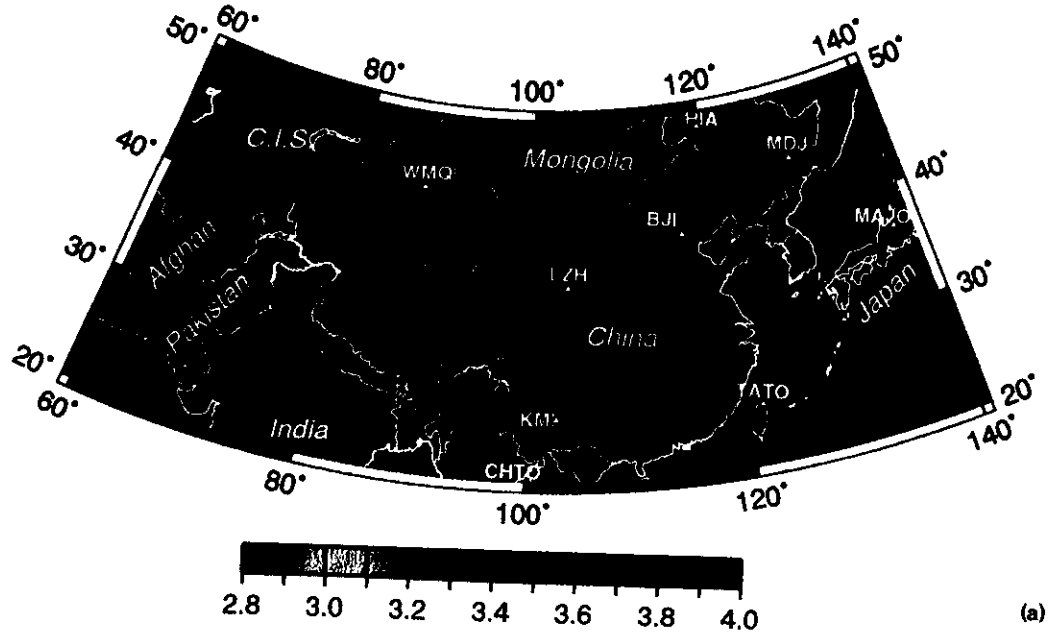

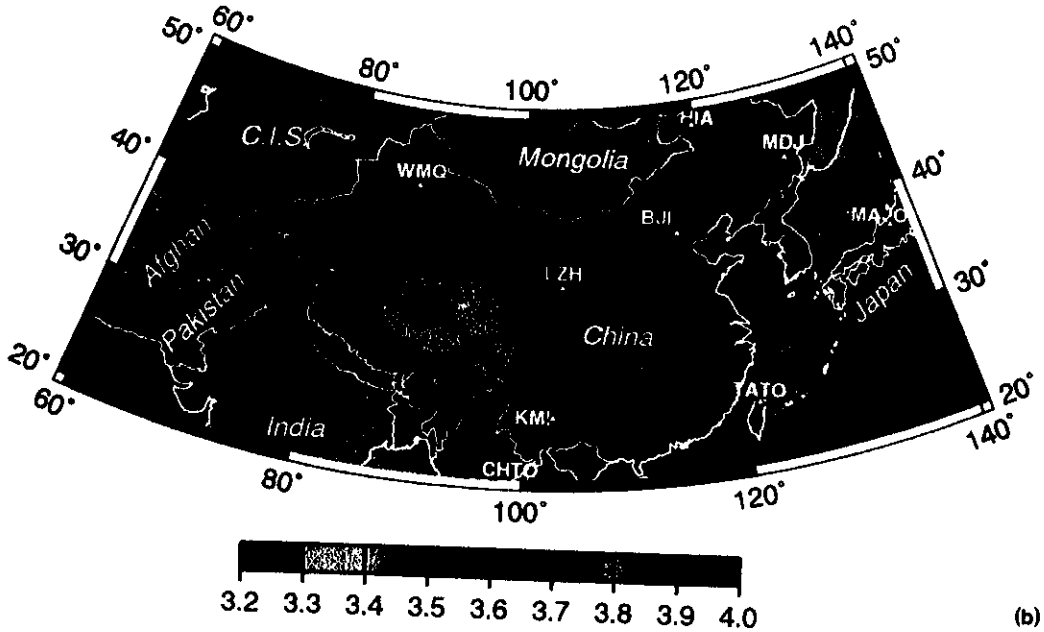

Fig. 5. Rayleigh wave group velocity tomographic inversion results for (a) 30 s, (b) 50 s, and (c) 70 s. (Note different scale for each figure.)

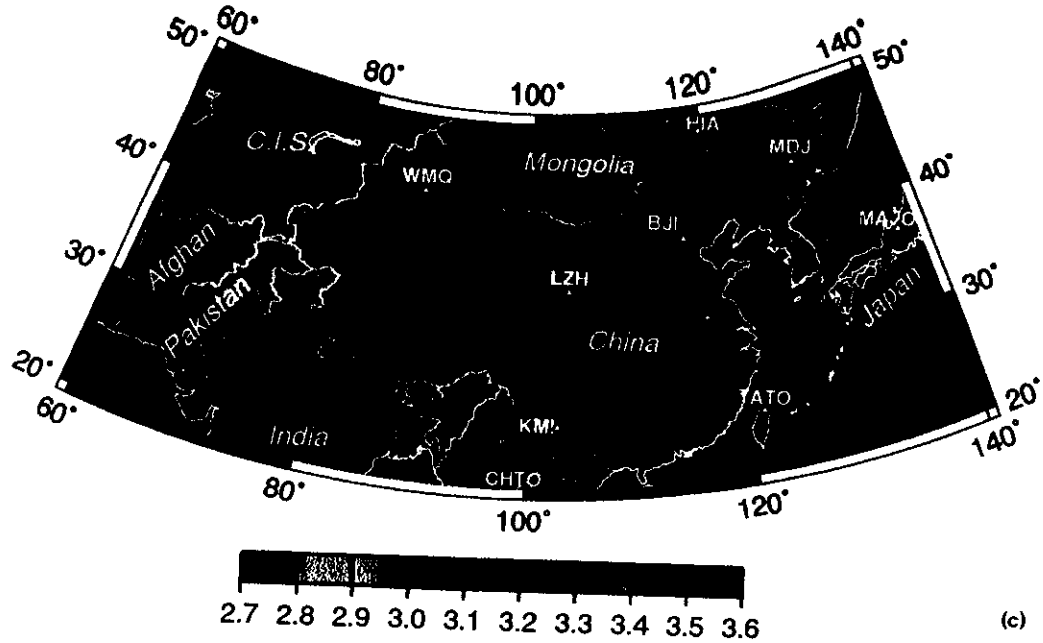

Fig. 5 (continued).

where

$$A^T = K^T(S + \alpha R_t)^{-1}$$

$$= \frac{1 - K^T(S + \alpha R_t)^{-1} t_0}{t_0^T(S + \alpha R_t)^{-1} t_0} t_0 (S + \alpha R_t)^{-1} \quad (10)$$

$$K_j(r) = \int_{L_j} \ln|r - r_j| \frac{ds_j}{U_0} \quad (11)$$

$$S_{ij} = \int_{L_i}\int_{L_j} \ln|r_i - r_j| \frac{dS_i}{U_0} \frac{dS_j}{U_0} \quad (12)$$

Space resolution is determined using the formula

$$R = \exp\left(\tfrac{3}{4} - A^T S A + 2K^T A\right) \quad (13)$$

Derivation of Eqs. (9)–(13) has been given by Ditmar and Yanovskaya (1987; see also Levshin et al. (1989).

The inversion proceeds by several steps:

(1) transformation from spherical coordinates θ, ϕ to Cartesian coordinates x, y is done by using the formulae (Yanovskaya, 1982; Jobert and Jobert, 1983)

$$x = R_0 \ln \tan(\theta/2)$$

$$y = R_0\phi$$

$$U(x, y) = U(\theta, \phi)/\sin\theta$$

where R_0 is the Earth's radius. This transformation does not distort a velocity distribution if the latitude θ is not very high. To make this transformation more accurate, the Earth's standard geocentric coordinate system is first transformed by rotation in such a way that the new equator crosses the middle of the territory under study and the new latitude range of wave paths is narrower than the real one. Several trials have demonstrated that reasonable variations of the new equator's position do not change the results of inversion.

(2) For each T_m the starting value of a group

velocity U_0 is found as an average along all paths

$$U_0 = \frac{\sum_{j=1,J} D_j}{\sum_{j=1,J} t_j}$$

Here D_j is a length of the path L_j.

(3) Functions $U(\theta, \phi)$ and $R(\theta, \phi)$ are found using Eqs. (9)–(13) and transformed to the initial coordinate system.

(4) Steps 2 and 3 are repeated with different values of the regularization parameter. There is

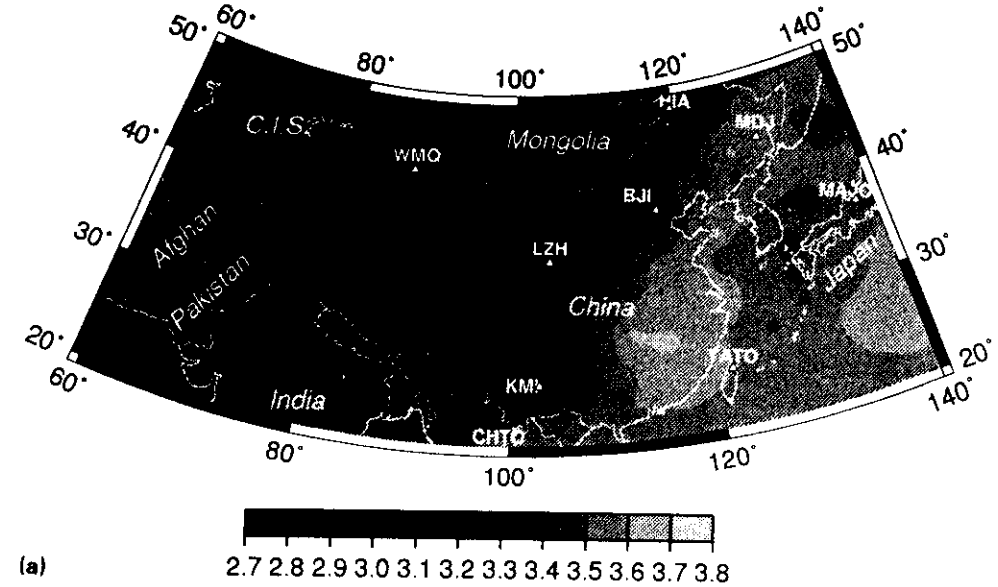

(a)

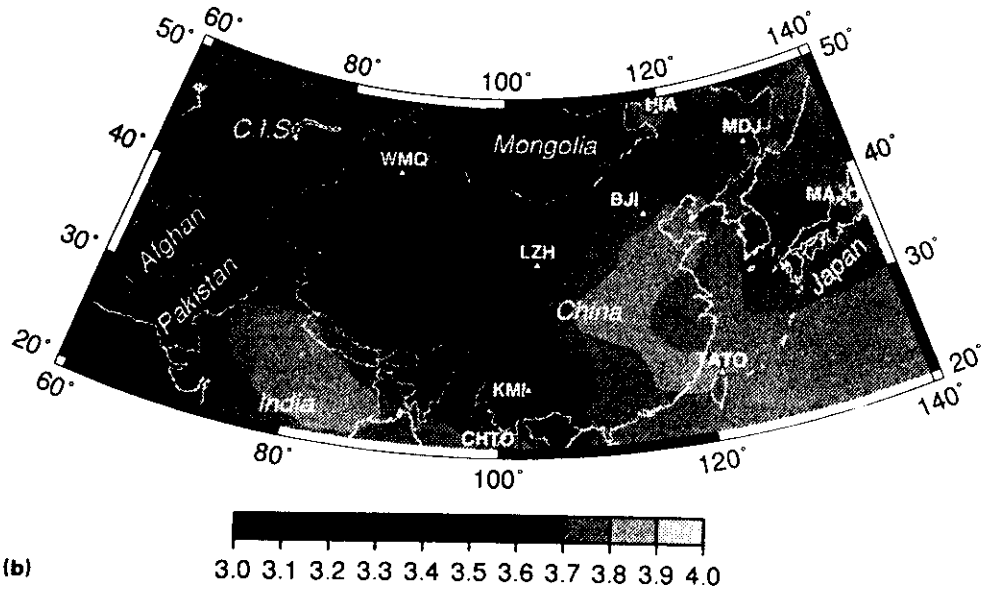

(b)

Fig. 6. Rayleigh wave group velocity tomographic inversion results for (a) 40 s and (b) 60 s. (Note different scale for each figure.)

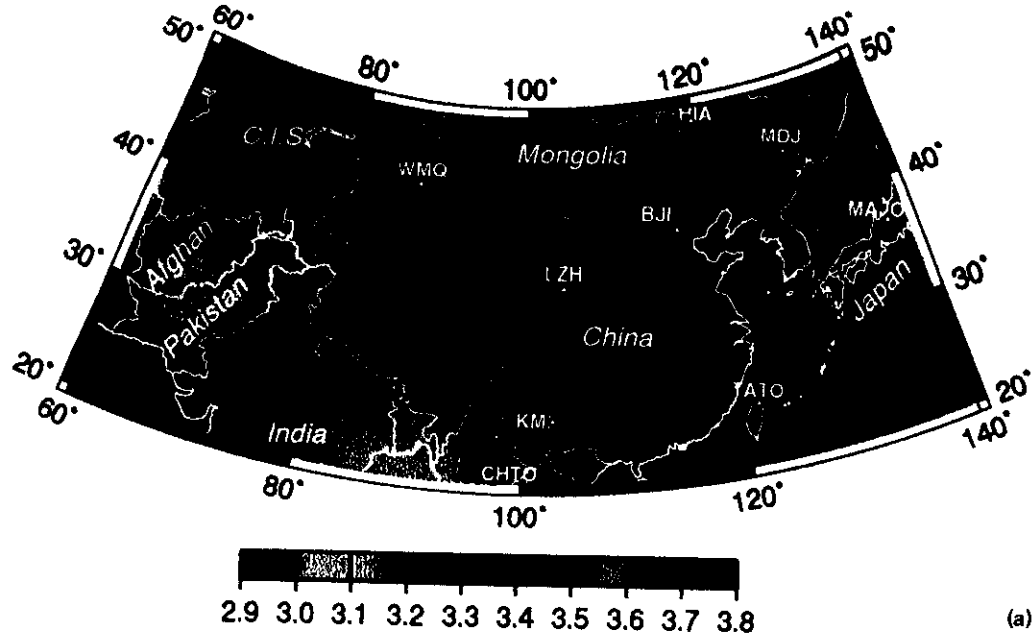

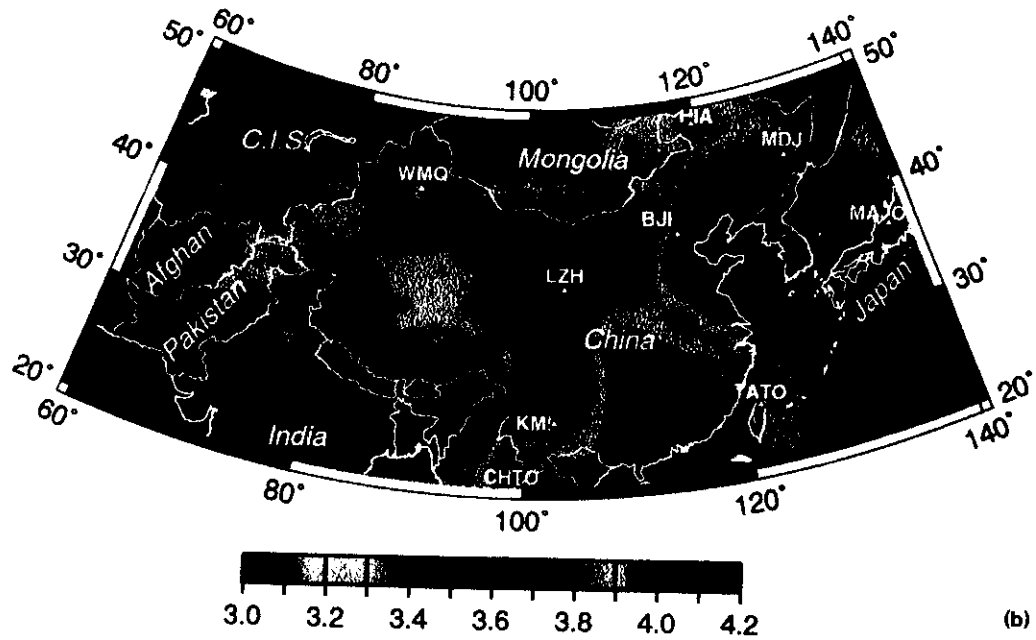

Fig. 7. Love wave group velocity tomographic inversion results for (a) 30 s, (b) 50 s and (c) 70 s. (Note different scale for each figure.)

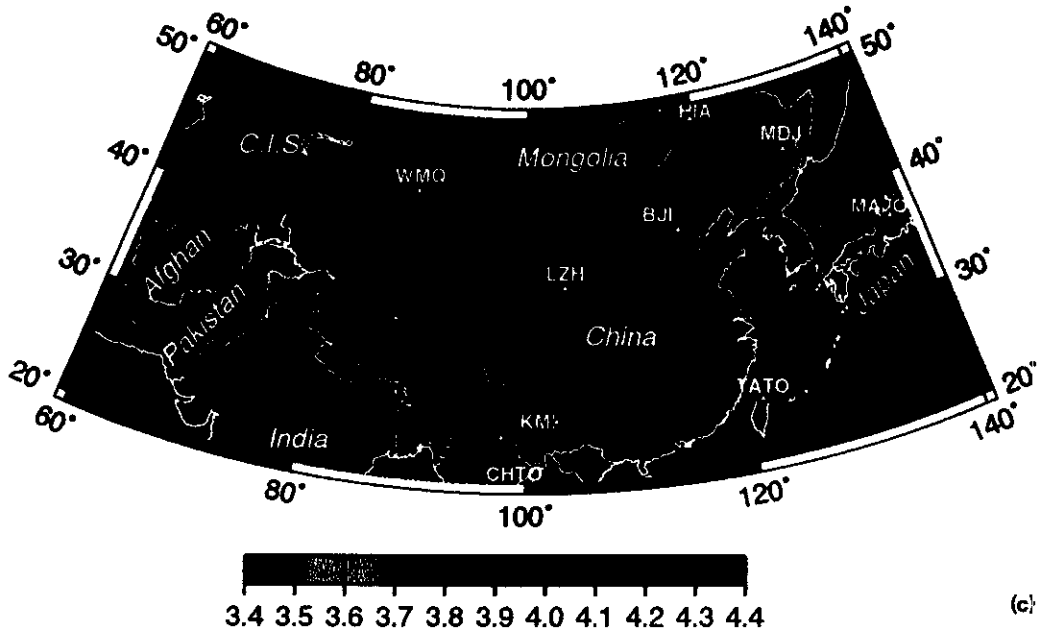

Fig. 7 (continued).

an option in the inversion procedure to take into account the presence of an azimuthal anisotropy in the Earth model. The group velocity model is constructed as a function of coordinates θ, ϕ and azimuth ψ

$$U_{\text{anis}}(\theta, \phi, \psi) = U(\theta, \phi)(1 - B \sin 2\psi)$$

U_{anis} is the anisotropic group velocity and the angle ψ and coefficient B are determined for each point.

4. Tomographic results

The path coverage we are able to obtain with our present dataset and the spatial resolution map for Rayleigh waves at 50 s are shown in Figs. 4(a) and 4(b), respectively. They are representative of the path coverage and resolution at other periods. The total number of paths used for each tomographic inversion, the corresponding initial group velocities and the mean square residuals for resulting models are presented in Table 1. Figs. 5(a)–5(c) and 6(a) and 6(b) show the tomographic results for Rayleigh waves at 30, 50, 70, 40, and 60 s periods. Figs. 7(a)–7(c), 8(a), and 8(b) show the tomographic results for Love waves at 30, 50, 70, 40, and 60 s periods. To maximize the color scale contrast for Figs. 5 and 7, we have chosen to set the minimum group velocity of each figure to red and the maximum to purple in the rainbow color scale; for gray scale maps (Figs. 6 and 8), we have used black for the minimum and light gray for the maximum. It should be noted that the areas covered by the topographic map (Fig. 1) and the Bouguer anomaly map (Fig. 2) are different from those of the tomographic images and the resolution maps, but with the aid of country boundaries and other markers, they can readily be compared. When viewing these maps it is important to keep in mind the following four factors. First, the resolution map, Fig. 4(b), indicates the spatial scales we can resolve in the various areas. For both Rayleigh and Love waves, the resolution length of our tomographic results is of the order of 450–700 km in the central part of the map and deteriorates sharply near the edge of the study area, where the path coverage is poor (Fig. 4(a)). Features smaller than the resolution length for a particular area tend to be

smeared. Second, as these are maps of group velocities, they cannot be interpreted directly in terms of differences in velocity structure; for example, low group velocities may arise from a combination of relatively low velocities in the vertical column and a thick crust. Third, the horizontal wavelengths corresponding to 30–70 s waves are approximately 95–280 km, and the images are expected to be smoother for longer periods. Finally, because Rayleigh and Love waves

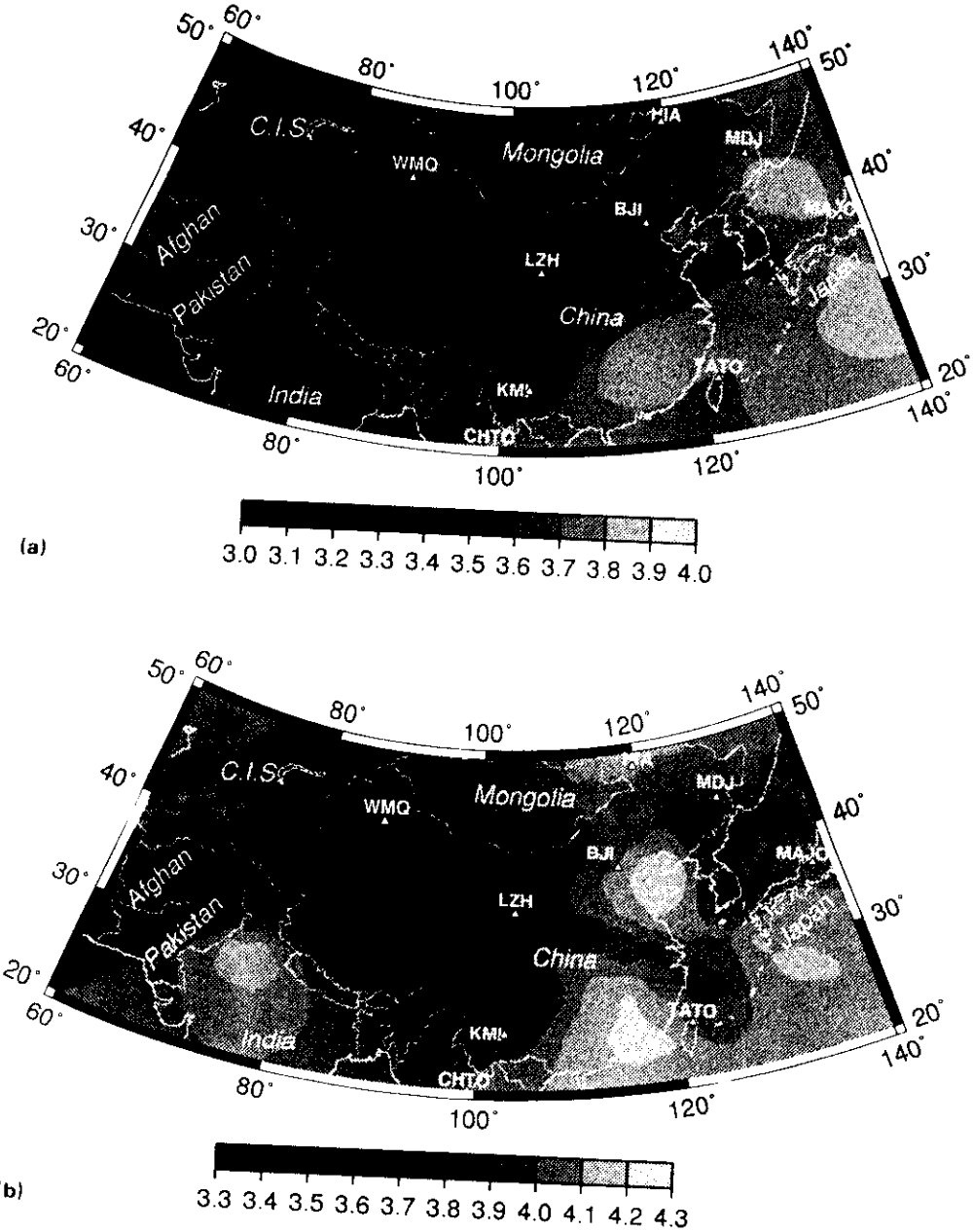

Fig. 8. Love wave group velocity tomographic inversion results for (a) 40 s and (b) 60 s. (Note different scale for each figure.)

have different eigenfunctions (Fig. 9), they sample the Earth differently even for an isotropic layered Earth; we do not expect the images for these two waves at the same period to be similar. All tomographic results were obtained assuming an isotropic model of the territory under study. Inversion experiments taking into account the presence of anisotropy result in a model with 2% variations of velocity with azimuth. The strike of the maximum velocity direction is 68°. This model produces practically the same group velocity maps and average residuals as the isotropic one. We conclude that the given set of data cannot resolve significant azimuthal anisotropy of surface-wave group velocities in the investigated regions.

The group velocity variations in the study area are remarkable. To facilitate our description of the maps, we shall divide this area into three sub-regions. Longitude 105°E can be used as the demarcation for the eastern and western regions of this study. There is a very noticeable change in topography along this line, from the western mountainous region to the plains of eastern China, and it corresponds roughly to the −100 mgal Bouguer gravity contour in Fig. 2, separating the region with high gradients and large negative anomalies from a region of relatively little change in anomalies (from −100 mgal to zero). Along the line, a sharp transition in group velocity exists, especially in the southern part (Figs. 5–8). We shall also subdivide the western region into southwestern and northwestern regions.

4.1. Tibet and southwestern region

In all the tomographic images (Figs. 5–8) the relatively low group velocities in the western part of the study area, when compared with those of the eastern part, are clearly seen. At 30 s, the Rayleigh image (Fig. 5(a)) exhibits an extensive low-velocity feature that covers the northern Tibetan plateau as well as a large portion of the western Tarim basin, the Pamirs, eastern Afghanistan, northern Pakistan and western Yunnan, west of Station KMI (Fig. 1). Some of these areas, for example, the western Tarim basin and northern Tibet, are known to have deep sedimentary covers. For Love waves at 30 s (Fig. 7(a)), the image looks very different; although the western Tarim remains a low-velocity feature, the Tibetan plateau has not yet emerged as a distinctive unit. The differences in Rayleigh and Love results can

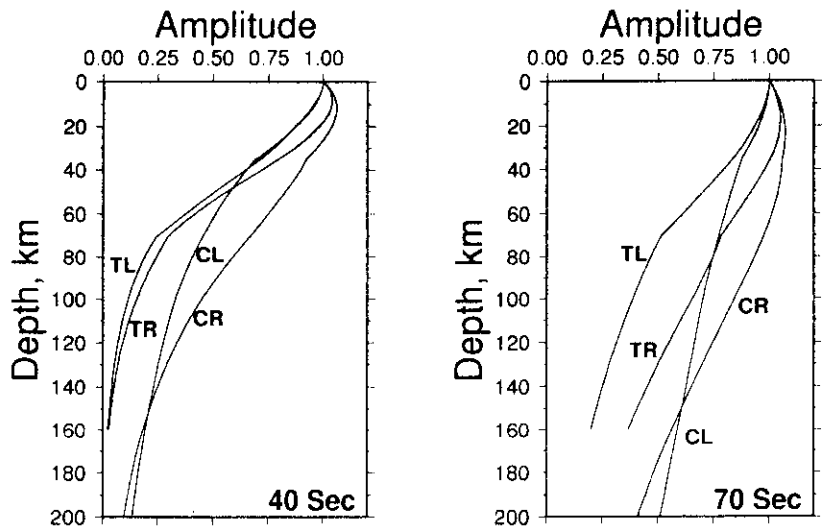

Fig. 9. Eigenfunctions for Rayleigh (R) and Love (L) waves at 40 s and 70 s for two extreme models: an approximate Tibet model (T) with a crust of 70 km thickness, and the Canadian Shield model (C) (Brune et al., 1963). TL, Tibetan Love wave; TR, Tibetan Rayleigh wave; CL, Canadian Shield Love wave; CR, Canadian Shield Rayleigh wave. For Rayleigh waves only the vertical (radial) eigenfunctions are shown.

be expected because of differences in eigenfunctions as noted above; Love waves sample shallower depth than do Rayleigh waves and the shallow part of the Tibetan plateau is not distinguishable from its neighboring areas.

By far the most prominent features in images for both Rayleigh and Love waves, at periods longer than 40 s, are the low group velocity closures that nearly coincide with the topographic Tibetan plateau (Figs. 5–8; see also Fig. 1). The area of lowest velocity for Rayleigh waves is at its maximum for 40 s and it continues to shrink for longer periods, with central Tibet as the core of low group velocity at 70 s. With the shear-wave velocities in the crustal and upper-mantle column probably being fairly similar across the plateau, the location of the group velocity minimum at 70 s signifies the fact that the crustal thickness is greater in eastern Tibet than in western Tibet. In most cases, the low-velocity closures extend to the Tarim and Qaidam basins. For Love waves, the closures are somewhat irregular in shape, but the area of low velocities still correlates well with the topography and the low-velocity area includes the Qaidam basin and a large part of the Tarim basin. In southern Tibet, near the suture, the Rayleigh velocity is relatively high. Although the spatial resolution of the images starts to deteriorate there, the area is covered by a number of paths, and the relatively high velocity there is most probably correct.

For Love wave tomography (Figs. 7(a)–7(c), 8(a), and 8(b), Tibet emerges as a recognizable feature with low group velocity for periods greater than 40 s. At 40 s period, the western Tarim, Pamirs and the Afghanistan–Pakistan low that dominates the tomographic image at 30 s is still clear. The Tibet low, however, becomes the dominant feature at 60 s and 70 s, with the overall shapes significantly different from that for Rayleigh waves. However, the Himalayas still appear as a higher-gradient zone and northwest India as a relatively high-velocity zone. The northwestern part of India, where the spatial resolution is about 1000 km (Fig. 4(b)), appears as a region of high group velocity for both Rayleigh and Love waves. This can clearly be seen for Rayleigh waves at 40–70 s (Figs. 5(b), 5(c), 6(a), and 6(b)) and for Love waves at 50–70 s.

4.2. Northwestern region

The Tarim basin is topographically well defined (Fig. 1) and is assumed to be underlain by Archean basement (Ren et al., 1986). It is often stated that the Tarim must be very rigid for it to remain undeformed while neighboring Tibet and the western Tienshan were subjected to enormous north–south strain. The area is seismically less active than the surrounding areas, as can be seen in Fig. 10. Gravitationally, it appears as a well-defined area of relatively high Bouguer anomalies (Fig. 2). It is therefore somewhat surprising that the Tarim, with its east–west dimension of the order of 1000 km and north–south width in excess of 500 km, does not show as a distinctive unit in the tomographic image, especially in view of the fact that the spatial resolution there is of the order of 500 km. In fact, as we pointed out above, the southwestern and western Tarim is a region of relatively low group velocity and forms a part of the Tibet low group velocity anomaly for Rayleigh and Love waves at 30, 40, 50, and 60 s (Figs. 5–8).

In the northwestern corner of our study area, there are relatively few paths in the region (Fig. 4(a)) and the spatial resolution is of the order of 1000 km. Tectonically, it is a part of the Altaids (Fig. 1). Figs. 5–8 show it as an area of relatively high velocity; it is particularly clear at 60 s and 70 s for Rayleigh waves (Figs. 5(c) and 6(b)). This area is not tectonically active at present, nor has it been active in the recent geological past.

The Tienshan is shown to taper from its western terminus in CIS Central Asia toward the east along the northern edge of the Tarim basin (Fig. 1). Southeast of WMQ, the Tienshan is fairly narrow with a mountain range in the north and a deep intermontane basin in the south. The seismicity map (Fig. 10) indicates that the eastern section, starting from just west of 90°E, is much less active than the western section. On many tectonic maps however (e.g. Terman, 1973), the eastern Tienshan and western Tienshan are not

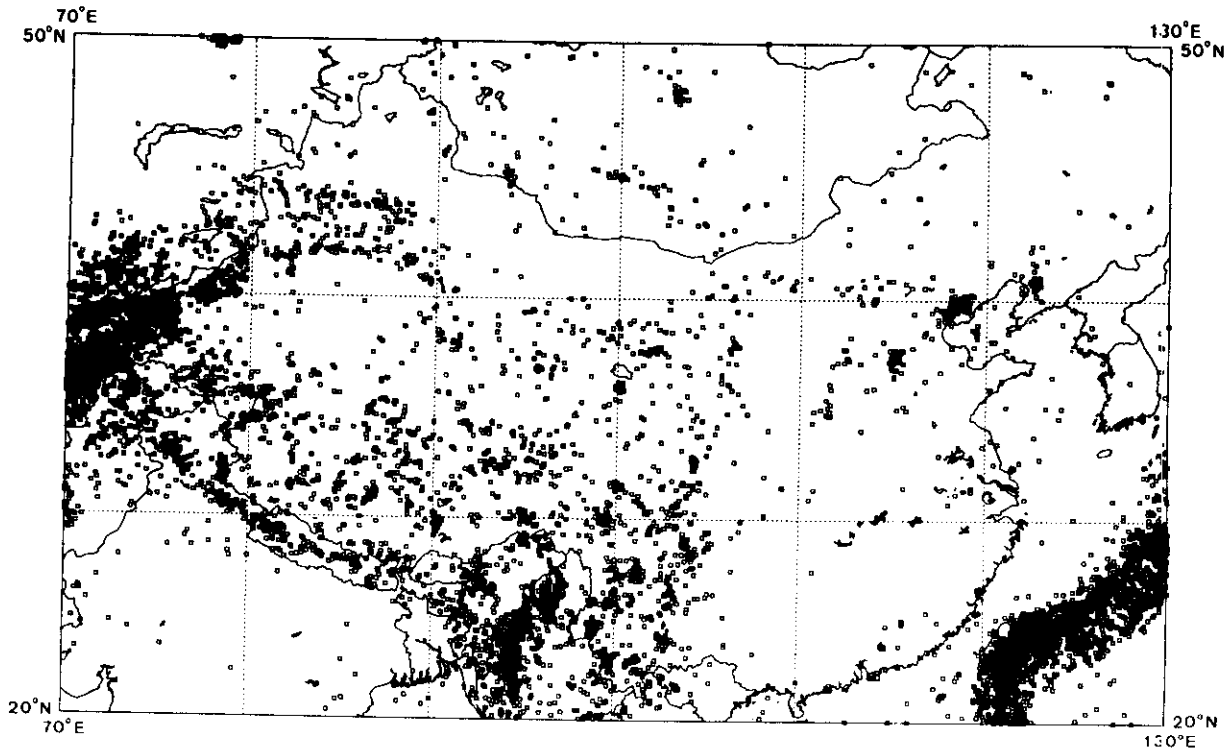

Fig. 10. Seismicity of the study area. Data include epicenters of all events of $M > 4$ from 1971 to 1992 published by the US Geological Survey in the Preliminary Determination of Epicenters (PDE).

distinguished. Our tomographic results show that the group velocities of Rayleigh and Love waves in the section of the Tienshan east of WMQ (Figs. 5–8) are relatively high. In particular, images of Rayleigh wave velocities at 40–70 s (Figs. 5(b), 5(c), 6(a), and 6(b)) and Love wave velocities at 30, 40, and 50 s (Figs. 7(a), 7(b), and 8(a)) show the transition rather well. It is also noticeable that a ridge of relatively high group velocity cuts diagonally across Mongolia, essentially along the extension of Lake Baikal, a modern rift structure (Molnar and Tapponnier, 1978).

4.3. Eastern region

The North China plain (Fig. 1) appears as a region with medium velocity at 30–50 s for both Rayleigh and Love waves, but at 60 s (Fig. 6(b)) the Bohai Gulf area east of BJI appears as a high-velocity region, and at 70 s (Fig. 5(c)) the whole North China plain becomes a very clear high-velocity region. Reflection and refraction profiles in this area (Wang and Mao, 1985) show that the crust is relatively thin, with the Moho at about 32 km depth; this is a sharp decrease from the crustal thickness of 40 km west of the 105°E longitude.

Much of the South China platform is a region of relatively high group velocity for Love waves at all periods and at 30–60 s for Rayleigh waves (Figs. 5–8); it is an area of low seismicity (Fig. 10). A low-velocity ridge, starting from the southern Ryukyus and continue northwestward along a portion of the southern boundary of the North China–Korean platform, seems to exist for Love waves at 50, 60, and 70 s (Figs. 7(b), 7(c), and 8(b)). This is an interesting feature that cannot easily be explained on the basis of surface geology or Bouguer gravity (Fig. 2).

It is interesting to note that the Ordos plateau is a region with very little seismicity, as shown in Fig. 10, and it is described also as a rigid block

surrounded by mobile belts (Ren et al., 1986). It does not appear in any of our images as a distint unit.

5. Discussion

The first-order tomographic images presented in this paper provide us with synoptic views of the lateral variability of the crust and upper mantle in East Asia. Many of the main tectonic units and topographic features (Fig. 1) can be distinguished reasonably well, but they appear to correlate better with the intensity of recent tectonic activity in each region. Our maps provide some quantitative measure of the deep crustal and upper-mantle structures under these features.

The Tibet–Pamir group velocity low dominates the tomographic images at periods greater than 40 s (Figs. 5(b), 5(c), 6(a) and 6(b)). In the case of a continental crust, such as that represented by the CANSD model (Brune and Dorman, 1963), Love and Rayleigh waves at 40 s or longer are most energetic as they travel through the upper mantle, and therefore sample that part of the mantle fairly well. However, for a Tibetan crust of 70 km (see Molnar, 1988, for a summary), Love and Rayleigh waves at 40 s are mostly trapped in the crust (Fig. 9). These contrasts in eigenfunctions are more pronounced at 70 s; at this period, the Tibetan–Pamir low still reflects the thick low-velocity crust, and the relatively high velocities in the eastern part of China result from thinner crust.

Judging from the distribution of group velocities in the Tibet–Pamir area, the crustal thickness is most probably greatest in the central part of Tibet. As it is extremely difficult to deploy stations in the Tibetan interior, tomographic imaging will probably provide the best chance to resolve the question of the lateral variations of structures within the plateau. Southern Tibet, near the Zangbo suture and the Himalayas, is a region of relatively high velocities, in comparison with the rest of the plateau. This result agrees with that of Jobert et al. (1985) obtained with instruments in southern Tibet. It is interesting that the Tibetan low velocity seems to extend under the southern Tarim basin, which is supposed to be a fairly rigid Precambrian block. The Tarim is not very active, seismically speaking, but the western part is known to have an east–west-oriented active thrust fault in the middle of the basin (Ren et al., 1986). Thus, although it might be a region with a geologically ancient basement, it is a currently active area.

The results we obtained for the Tibet–Pamir plateau are similar to those shown in Bourjot and Romanowicz's (1992) tomographic study, using only Rayleigh waves. Similar low-velocity features are seen to persist up to 60 s in their work; in our Rayleigh wave results we see this clearly even at 70 s (Fig. 6(c)), although the area is smaller than at shorter periods.

We have noted above that the Tienshan fold belt east of longitude 87°E (Fig. 1) is noticeably distinct from the western part in that, whereas the western part reveals itself as an area with low Rayleigh wave group velocity, the eastern part is an area of higher velocity. This feature seems to be consistent with the observation that the Bouguer gravity low (Fig. 2) associated with the western Tienshan (the −250 mgal contour) terminates there. Also, the Tienshan here is actually a east–west-striking basin and range province, with the sub-sea-level Turfan basin as the lowest point. Evidently, this is a deep-seated feature, with a thin crust underneath, resulting perhaps from north–south tension. The seismicity of the western section of the Tienshan is rather high, with large thrust events; in contrast, the eastern Tienshan has low seismicity (Fig. 10).

The increase in group velocities of both the Rayleigh and Love waves eastward across 105°E is clear in Figs. 5–8. The trend agrees generally with that shown in the Bouguer gravity map (Fig. 2). In the eastern half of the study area, the relatively high velocity region south and east of Beijing (the North China plain) is easily distinguished; it is evidently related to the thin crust (generally less than 35 km) in that region (Wang and Mao, 1985). The North China plain is a region of active extensional tectonics (Nabelek et al., 1987) where many large earthquakes have occurred. Our group velocity maps show that this region may extend to areas across the Bohai Gulf,

east of BJI or even to the Sung-Liau Plain (Figs. 1, 5(c) and 7(c)).

Southeastern China is also a region of relatively high velocities, especially at periods less than 70 s. Here the thin Archaen crust (about 32 km; Wang and Mao, 1985) is probably the main controlling factor. In contrast to the North China plain, this region is not tectonically active. The Japan Sea area appears as a high-velocity region for Love and Rayleigh waves at 40 s (Figs. 6(a) and 8(a)), but becomes an area of relatively low velocity for longer-period Rayleigh waves (Figs. 6(d) and 6(e)).

6. Conclusion

The results of this surface-wave tomographic inversion study provide clear images of the variable nature of the deep crustal and upper-mantle structures under eastern Asia as a whole. We are able to correlate many of the features in the group velocity maps with regional tectonics. It is clear that, in contrast to observations in some shield areas of the world (e.g. Snieder, 1988), the Precambrian basement rocks, such as those of the Tarim basin, do not seem to be underlain by high-velocity crust and upper mantle. The surface-wave tomographic technique is evidently a powerful one for this region, where only a few high-quality digital seismic stations exist and where there are a large number of moderate to strong earthquakes in and around the study area. To further refine the group velocity maps, it is necessary to consider curved wave paths in future work, as the velocity gradients we see in these images are rather high, with total group velocity changes of the order of $\pm 15\%$ in the study area.

Acknowledgments

This study was supported by Air Force Phillips Laboratory Contract F1962890K0042 and NSF Grant EAR9004220. We are grateful to Drs. T. Yanovskaya and P. Ditmar from the University of St. Petersburg, Russia, for providing us with their tomographic inversion program. We thank Dr. P. Wessel, who distributes freely his GMT software. We also thank Dr. E. Fielding for providing digital map data. At various stages of this work, graduate students at SUNY Binghamton assisted ably; we would like to mention especially D. Salzberg, Y.L. Kung, and R.J. Rau. We also thank B. Hutt of Albuquerque Seismic Laboratory (ASL), US Geological Survey, for giving us a copy of his instrument response program.

References

Backus, G. and Gilbert, F., 1968. The resolving power of gross Earth data. Geophys. J.R. Astron. Soc., 16: 169–205.

Backus, G. and Gilbert, F., 1970. Uniqueness in the inversion of inaccurate gross Earth data. Philos. Trans. R. Soc. London, 226: 123–192.

Bourjot, L. and Romanowicz, B., 1992. Crust and upper mantle tomography in Tibet using surface waves. Geophys. Res. Lett., 19: 881–884.

Brandon, C. and Romanowicz, B., 1986. A 'no-lid' zone in the central Chang-Thang platform of Tibet: evidence from pure path phase velocity measurements of long period Rayleigh waves. J. Geophys. Res., 91: 6547–6564.

Brune, J.N. and Dorman, J., 1963. Seismic waves and Earth structure in the Canadian Shield. Bull. Seismol. Soc. Am., 53: 167–210.

Chun, K.Y. and Yoshii, T., 1977. Crustal structure of the Tibetan Plateau: a surface wave study by a moving window analysis. Bull. Seismol. Soc. Am., 67: 737–750.

Ditmar, P.G. and Yanovskaya, T.B., 1987. A generalization of the Backus–Gilbert method for estimation of lateral variations of surface wave velocity. Izv. Akad. Nauk SSSR, Fiz. Zemli, 6: 30–60.

Feng, C.C. and Teng, T., 1983. Three-dimensional crust and upper mantle structure of the Eurasian continent. J. Geophys. Res., 88: 2261–2272.

Feng, R., Zhu, J.S., Ding, Y.Y., Chen, G.Y., He, Z.Q., Yang, S.B., Zhou, H.N. and Sun, K.Z., 1983. Crustal structure in China from surface waves. Chin. Geophys. Am. Geophys. Union, 2: 273–289.

Hirn, A., 1988. Features of the crust–mantle structure of Himalayas–Tibet: a comparison with seismic traverses of Alpine, Pyrenean and Variscan orogenic belts. Philos. Trans. R. Soc. London, Ser. A, 327: 17–32.

Jobert, N. and Jobert, G., 1983. An application of the ray theory to the propagation of waves along a laterally heterogeneous spherical surface. Geophys. Res. Lett., 10: 1148–1151.

Jobert, N., Jounet, B., Jobert, G., Hirn, A. and Sun, K.Z., 1985. Deep structure of southern Tibet inferred from the dispersion of Rayleigh waves through a long-period seismic network. Nature, 313: 386–388.

Kozhevnikov, V.M. and Barmin, M.P., 1989. Dispersion curves of Rayleigh wave group velocities for several regions of the Asian continent. Izv. Akad. Nauk SSSR, Fiz. Zemli, 9: 16–25.

Kozhevnikov, V.M., Lokshtanov, D.E. and Barmin, M.P., 1992. Shear-velocity structure of the lithosphere for nine large tectonic regions of the Asian continent. Izv. Akad. Nauk SSSR, Fiz. Zemli, 1: 61–70.

Levshin, A.L., Yanovskaya, T.B., Lander, A.V., Bukchin, B.C., Barmin, M.P., Ratnikov, L.I., et al.,0 1989. In: V.I. Keilis-Borok (Editor), Seismic Surface Waves in a Laterally Inhomogeneous Earth. Kluwer Academic, Dordrecht, 293 pp.

McCowan, D.W. and Lacoss, R.T., 1978. Transfer functions for the Seismic Research Observatory seismograph systems. Bull. Seismol. Soc. Am., 68: 501–512.

Molnar, P., 1988. A review of geophysical constraints on the deep structure of the Tibetan Plateau, the Himalaya and the Karakoram and their tectonic implications. Philos. Trans. R. Soc. London, Ser. A, 327: 33–88.

Molnar, P. and Tapponnier, P., 1978. Active tectonics of Tibet. J. Geophys. Res., 83: 5361–5375.

Nabelek, J., Chen, W.P. and Ye, H., 1987. The Tangshan earthquake sequence and its implications for the evolution of the North China Basin. J. Geophys. Res., 92: 12615–12628.

Patton, H., 1980. Crustal and upper mantle structure of the Eurasian continent from the phase velocity and Q of surface waves. J. Rev. Geophys. Space Phys., 18: 605–625.

Ren, J.S., Jiang, C.F., Zhang, Z.K. and Qin, D.Y., 1986. Geotectonic Evolution of China. Springer, New York, 203 pp.

Sengor, A.M.C., Natal'in, B. and Burtman, K., 1993. Evolution of the Altaid tectonic collage and Palaeozoic crustal growth in Eurasia. Nature: 364: 299–307.

Snieder, R., 1988. Large-scale waveform inversions of surface waves for lateral heterogeneity, 2. Application to surface waves in Europe and the Mediterranean. J. Geophys. Res., 93: 12067–12080.

Terman, M., 1973. Tectonic map of China and Mongolia. Geol. Soc. Am., Boulder, CO, scale 1:5000000.

Tikhonov, A.N. and Arsenin, V., 1976. Méthodes de Résolution de Problèmes mal posés. MIR, Moscow, 233 pp.

US Air Force (USAF), 1971. Bouguer gravity anomaly map of Asia. Aeronautical Chart and Information Center, St. Louis, MO, scale 1:9000000.

Wang, G.Z. and Mao, E.T. (Editors), 1985. Crust and Upper Mantle in China, Results of Geophysical Exploration. Seismological Press, Beijing, 407 pp.

Wier, S., 1982. Surface wave dispersion and Earth structure in South-Eastern China. Geophys. J.R. Astron. Soc., 69: 33–47.

Wu, F.T., 1978. Recent tectonics of Taiwan. J. Phys. Earth, 26(Suppl.): S265–S299.

Yanovskaya, T.B., 1982. Distribution of surface wave group velocities in the North Atlantic. Izv. Akad. Nauk SSSR, Fiz. Zemli, 2: 3–11.

Yanovskaya, T.B. and Ditmar, P.G., 1990. Smoothness criteria in surface wave tomography. Geophys. J. Int., 102: 63–72.

Note to contributors

The Editors invite colleagues who are preparing papers within the scope of the Journal to submit them for publication. Please note that the manuscripts should be written in the English language. A detailed *Guide for Authors* is available on request, and is also printed in Vol. 82, No. 1, pp. 83–86. You are kindly requested to consult this guide.

Letter Section

The *Letter Section* is entirely devoted to short manuscripts describing preliminary results, suggestions for new applications of analytical methods, new theories, etc.

Communications intended for this PEPI Letter Section should not exceed six printed pages and should be self-contained. The manuscripts received will be published *not later than three months* after their final acceptance.

Manuscripts should contain a brief summary of approx. 50 words. In order to achieve rapid publication, no proofs will be sent to the authors. Manuscripts should therefore be prepared with the greatest possible care.

Preparation of the text

(a) The manuscript should be typewritten with double spacing and wide margins and include, at the beginning of the paper, an abstract of not more than 500 words. Words to be printed in italics should be underlined. The S.I. unit system should be used throughout.

(b) The title page should include: the title, the name(s) of the author(s) and their affiliations, in that order.

References

(a) References in the text start with the name of the author(s), followed by the publication date in parentheses.

(b) The reference list should be in alphabetical order and on sheets separate from the text, in the following style:

Bullen, K.E., 1975. The Earth's Density. Chapman and Hall, London, 420 pp.

Kanamori, H. and Cipar, J.J., 1974. Focal processes of the great Chilean earthquake May 22, 1960. Phys. Earth Planet. Inter., 9: 128–136.

Knopoff, L., 1972. Model for the aftershock occurrence. In: H.C. Heard, I.Y. Borg, N.L. Carter and C.B. Raleigh (Editors), Flow and Fracture of Rocks. Am. Geophys. Union, Geophys. Monogr. Ser., 16: 259–263.

Toksoz, M.N., Thomson, K.C. and Ahrens, T.J., 1971. Generation of seismic waves in prestressed media. Bull. Seismol. Soc. Am., 61: 1589–1623.

Names of journals should be abbreviated according to the *Bibliographic Guide for Editors*, published by the American Chemical Society, Washington, DC, USA.

Tables

Tables should be compiled on separate sheets. A title should be provided for each table and they should be referred to in the text.

Illustrations

(a) All illustrations should be numbered consecutively and referred to in the text.

(b) Drawings should be completely lettered, the size of the lettering being appropriate to that of the drawings, but taking into account the possible need for reduction in size (preferably not more than 50%). The page format of the Journal should be considered in designing the drawings.

(c) Photographs must be of good quality, printed on glossy paper.

(d) Figure captions should be supplied on a separate sheet.

Proofs

One set of proofs will be sent to the author, to be carefully checked for printer's errors (the publisher does not read proofs). In the case of two or more authors please indicate to whom the proofs should be sent.

Page charges and reprints

There will be *no page charge*. Each author receives with his proofs a reprint order form which must be completed and returned to the Publisher with the proofs. *Fifty reprints* of each article are supplied *free of charge*.

Submission of manuscript

Manuscripts should be submitted in triplicate to one of the three Editors, whose addresses are listed on the front inside cover. Illustrations should also be submitted in triplicate. One set should be in a form ready for reproduction; the other two may be of lower quality.

Submission of electronic text

In order to publish the paper as quickly as possible after acceptance authors are encouraged to submit the final text also on a 3.5" or 5.25" diskette. Both double density (DD) and high density (HD) diskettes are acceptable. However, the diskettes should be formatted according to their capacity (HD or DD) before copying the files onto them. Similar to the requirements for manuscripts submission, main text, list of references, tables and figure legends should be stored in separate text files with clearly identifiable file names. The format of these files depends on the wordprocessor used. Texts made with DisplayWrite, MultiMate, Microsoft Word, Samna Word, Sprint, TeX, Volkswriter, Wang PC, WordMARC, WordPerfect, Wordstar, or supplied in DCA/RFT, or DEC/DX format can be readily processed. In all other cases the preferred format is DOS text or ASCII. It is essential that the name and version of the wordprocessing program, type of computer on which the text was prepared, and format of the text files are clearly indicated. The final manuscript may contain parts (e.g. formulae, complex tables) or last minute corrections which are not included in the electronic text on the diskette; however, these should be clearly marked on an additional hardcopy of the manuscript.

Books for review should be addressed to: Editorial Office Earth Sciences, Elsevier Science B.V., P.O. Box 1930, 1000 BX Amsterdam.

Submission of an article is understood to imply that the article is original and unpublished and is not being considered for publication elsewhere.

Upon acceptance of an article by the journal, the author(s) resident in the USA will be asked to transfer the copyright of the article to the publisher. This transfer will ensure the widest possible dissemination of information under the US Copyright Law.

0031-9201/94/$07.00